TECHNICAL PAPER

Influence of streamwise position of crescent-shaped block on flat-plate film cooling characteristics

Chao Zhang[1,2] · Zhan Wang[3]

Abstract

Film cooling injection from discrete circular holes is widely used in gas turbines to reduce the heat load of the turbine blades. Placing a special designed structure upstream or downstream, the circular hole has been proven to be a new effective way to improve cooling effectiveness in recent years. In the present study, numerical investigations were performed on a row of circular holes over a flat plate with crescent-shaped blocks. Totally seven configurations without block, with blocks located at six streamwise positions including 6 times, 5 times, 4 times of hole diameter upstream, and 0.5 times, 1.5 times, 2.5 times of hole diameter downstream at blowing ratios of 0.5–1.5 were tested symmetrically. The Reynolds-averaged Navier–Stokes equations with the k–ω shear-stress transport model were solved. Flow fields, cooling effectiveness and aerodynamic losses were analyzed in detail. Although with different generation mechanism, additional vortex pair opposite to the counter-rotating vortex pair was generated by placing either an upstream or downstream block, which could finally improve the coolant lateral coverage and thus cooling effectiveness. The cooling performances and aerodynamic losses between configurations without block and with blocks at six streamwise positions were then compared. Finally, the optimal streamwise position of the block was recommended at various blowing ratios.

Keywords Gas turbine · Film cooling · Crescent-shaped block · Streamwise position · Cooling effectiveness · Aerodynamic loss

1 Introduction

Film cooling is one of the most common used methods to reduce the heat load of the gas turbine blades in order to enable higher turbine inlet temperature. In a typical film cooling configuration, the coolants extracted from the compressor are effused through a set of discrete inclined holes and then form a thin protective layer between the blade surfaces and the mainstream hot gas. However, consumption of the coolants with high pressure represents some work loss for the gas turbine. Hence, numerous researches have been devoted to understand the fundamental physics of the film cooling and further improve the cooling performance. It is well known that the interaction between the coolant and the mainstream hot gas leads to complicated flow structures that lead to mixing loss and a decay of cooling performance. Fric and Roshko [1] experimentally studied the flow field downstream a circular hole and found that the counter-rotating vortex pair (CRVP) plays a key role to cause the "lift-off" of the ejected coolants. The CRVP with stronger intensity at high blowing ratios could dramatically decrease the coolant converge and the cooling performance. An et al. [2] proposed that less numbers of cooling holes are required to operate at higher blowing ratios in order to simplify blade manufacturing. Therefore, developing film cooling hole with high efficiency at high blowing ratios are imperative.

In the past few decades, the most important achievement on film cooling was the application of shaped hole for both heavy and aircraft gas turbines [3]. In comparison

✉ Chao Zhang
  czhangxj83@163.com

1 Tianjin Key Laboratory for Advanced Mechatronic System Design and Intelligent Control, School of Mechanical Engineering, Tianjin University of Technology, Tianjin, China

2 National Demonstration Center for Experimental Mechanical and Electrical Engineering Education (Tianjin University of Technology), Tianjin, China

3 School of Energy and Power Engineering, Shandong University, Jinan, China

with the circular hole, the intensity of CRVP of shaped hole was weaken obviously due to lower momentum flux of the ejected coolants and the larger hole exit area. Therefore, the shaped hole yielded lower penetration into the mainstream hot gas, better lateral spreading and improved cooling effectiveness. The benefit of shaped hole is more pronounced at high blowing ratios. But the drawback of shaped hole is that the manufacturing cost is significantly higher than the circular hole.

In contrast with the geometrical complicated shaped hole, many researchers focused on the modifications based on the simple circular hole. Kusterer et al [4] proposed the so-called double-jet hole configuration combining two rows of circular holes with laterally inclined angles at opposite locations along the streamwise direction. The double-jet hole configuration results in a more or less symmetrical vortex pair to counteract the CRVP. Heidmann and Ekkad [5] presented the anti-vortex hole configuration consisting of additional two small circular holes on sideways. The ejected coolants from the two side holes generate additional vortices, which are opposite to the CRVP and thereby suppress the coolants to be attached to the blade surfaces.

Unlike the utilization of extra circular holes in [4, 5], Nasir et al. [6] placed a triangular tab along the upstream edge of the circular hole exit and found that additional vortex pair generated by the tab can reduce the coolant penetration and thus increase cooling effectiveness. But they also pointed out that the tab configuration may be more difficult to manufacture because of the coverage of part of the hole exit. Na and Shih [7] placed a backward-facing ramp upstream the hole and found the approaching boundary layer is deflected and the horseshoe vortex is eliminated. Zheng et al [8] evaluated the effects of a divided transverse step upstream the hole and found that the coolant penetration can be reduced and additional vortices opposite to the CRVP are generated. Kawabata et al. [9] proposed the concept of flow control device with a half ellipse-shaped protrusion upstream the hole. It was experimentally verified that the hairpin vortex generated by the flow control device promotes the attachment of downstream coolant jet. Kawabata et al. [10] further evaluated the flow control device attached to a linear vane cascade model. Their experimental and numerical results in [10] both showed that the induced streamwise vortices suppress the coolant jet to be attached to the surface, and vortices with opposite rotation direction against the CRVP improve the coolant spreading in lateral region. Sarkar and Ranakoti [11] numerically investigated the effect of down-wash and up-wash-typed vortex generator pairs with two opposite laterally oriented plates upstream the hole. The down-wash vortex generators generated the additional vortex pair to weaken the CRVP resulting in better cooling effectiveness, but the up-wash vortex generators augmented the CRVP resulting in poor cooling effectiveness. Zhou

and Hu [12] proposed a novel structure with the shape of barchan dune upstream the hole and experimentally verified the availability of weakening the CRVP by the downstream barchan dune shell.

Different from the above-mentioned configurations [7–12] upstream the hole, the effects of the various shaped blocks or vortex generators downstream the hole were also studied by several researchers. Zaman et al [13] investigated the effects of delta-shaped vortex generator on the downstream flow field. Their experimental results showed that the vortex generator appears to be effective in keeping the jet attached to the wall. Shinn and Varkan [14] analyzed in detail the vortex structures downstream the circular hole with a downstream micro-ramp vortex generator by using large eddy simulation (LES) method. It was found that the downstream vortex generator can improve cooling effectiveness by generating near-wall vortices opposite to the CRVP. The experimental work by Song et al. [15] also revealed the down-wash effect of the induced vortices by the delta-shaped vortex generator at blowing ratios ranging from 0.5 to 1.5. In order to expand the lateral coolant coverage and alter the vortex structure around the hole, An et al. [16] proposed a streamlined crescent-shaped block downstream the hole. The experimental results showed that the cooling effectiveness can be improved at blowing ratios ranging from 0.5 to 1.25. The crescent-shaped block downstream the hole was also numerically evaluated by Khorsi et al. [17].

In spite of improved cooling effectiveness with upstream or downstream structure, additional aerodynamic loss will be generated due to the violent mixing. The aerodynamic measurement by Barigozzi et al. [18] with a ramp upstream validated the above viewpoint. Obviously, the cooling performance and aerodynamic loss are affected by the specific geometry and the location of the block. In the review of the literature [7–17], several specific block shapes were opposed. Except for the block shape [7–17], the height of the block also has a great impact on the cooling performance and aerodynamic loss. Based on the results in [9–11], higher protrusions or vortex generators upstream the hole resulted in better cooling performance but also higher aerodynamic loss. The experimental studies in [12, 13, 16] for the downstream vortex generators also gave the similar conclusions. Zhang et al. [19] focused on the effect of the downstream delta vortex generator height on cooling performance at blowing ratio of 1.5 and found an optimal height exists for maximum area-averaged cooling effectiveness. Zhang and Wang [20] suggested the optimal height of the downstream crescent-shaped block with highest cooling performance at either blowing ratio ranging from 0.5 to 2.0. Besides, the specific streamwise position of the block has great influence in principle. Based on the authors' knowledge, up to now, there are only a few studies [13, 21] focusing on the effect of the streamwise position of the block. The experimental

results in [13] showed that the streamwise location has little influence on the flow field when the distance between the vortex generator to the hole exit is larger than 3 times of hole diameters. For the crescent-shaped block downstream the hole, An et al. [16] found that the distance between the block and the hole exit, ranged from 0.25 times to 0.75 times of the hole diameter, has little impact on the cooling performance at blowing ratios of 0.5, 0.75 and 1.0, but obvious influence at a blowing ratio of 1.25. Zhou and Hu [21] compared the cooling effectiveness with the upstream and downstream dune-shaped structures located at four streamwise positions and founded that the configuration just upstream the hole shows best cooling effectiveness. But the aerodynamic loss was not discussed for blocks with different streamwise positions in [16, 21].

Due to the relatively simple geometry and competitive cooling performance, as compared with the highly three-dimensional barchan dune in [12, 21], the crescent-shaped block proposed by An et al. [16] is focused in present study. Present paper aims to numerically investigate the effects of the crescent-shaped block streamwise position for configuration with a row of circular holes on the cooling performance and the aerodynamic loss. The streamwise distance between the hole exit and the crescent-shaped block varies from -6 times to 2.5 times of the hole diameter, and the blowing ratios are 0.5, 1.0 and 1.5. The flow fields, cooling effectiveness and aerodynamic losses are analyzed and compared for the configurations without block and with blocks at different streamwise positions at three blowing ratios.

2 Computational model and numerical details

2.1 Computational model

Figure 1 describes the sketch of the computational model with specific geometry dimensions. Note that the computational domain is the same as that in the work of [20], except for the crescent-shaped block with different streamwise positions.

The computational model consists of a rectangular mainstream hot gas channel, a circular cooling hole connected with a coolant plenum chamber, and a crescent-shaped block (not shown in Fig. 1a). The original point of coordinates is set at the intersection point of the hole trailing edge and the wall. The coordinates X, Y and Z represent the streamwise, vertical and lateral directions, respectively. The circular cooling hole has a diameter D of 8 mm, a length-to-diameter L/D of 6.25, a pitch in the lateral direction of $3D$, and an inclination angle of 30° to the streamwise direction. The inlet of the mainstream channel is set at $30D$ upstream of the trailing edge of the hole, whereas the outlet is at $50D$

downstream. The upper wall of the mainstream channel is set at a distance of $15.625D$ away from the bottom wall in the vertical direction. The coolant plenum chamber has a cross section of $15D \times 3D$ and a height of $15.625D$. The specific geometry dimensions of the crescent-shaped block are illustrated in Fig. 1b. The block has a height H/D of 0.5 in the vertical direction, a length of $1.5D$ in the streamwise direction, and a width of $2.0D$ in the lateral direction. The distance between the leading edge and trailing edge of the block in the streamwise direction is $0.75D$. The block dimensions are all fixed except for the streamwise position. In order to investigate the effect of the block streamwise position, six typical distances between the tailing edge of the hole and the leading edge of the block L_c in streamwise direction are shown in Fig. 1c. The values of the streamwise distances are set to be $-6D$, $-5D$, $-4D$, $0.5D$, $1.5D$ and $2.5D$, respectively. In the following study, model 1 represents the cooling hole configuration without block, models 2–4 represent the configurations with upstream blocks of $L_c = -6D$, $-5D$ and $-4D$, and models 5–7 represent the configuration with downstream block of $L_c = 0.5D$, $1.5D$ and $2.5D$.

2.2 Numerical method

The investigations of film cooling have been carried out by using the commercial software ANSYS CFX with steady-state simulations. The Reynolds-averaged Navier–Stokes equations (RANS) are selected to solve because of the less computational cost than the LES method performed in [14]. Then, the k–ω-based shear-stress transport (SST) two-equation turbulence model is selected to compute the averaged turbulent stresses, due to its accurate prediction capability in film cooling performance [20]. The advection and turbulence terms are both solved with high resolution schemes. When the root mean square residuals of all variables are less than 10^{-6} and variation of the velocity in vertical direction at the hole exit is less than 0.01 m/s, the simulations are regarded to achieve convergence.

2.3 Boundary condition

In present study, the operating conditions are similar with the experimental conditions in An et al [16]. Ideal airs are used for mainstream hot gas and coolant in plenum chamber. The freestream velocity U_m and turbulence intensity at the inlet of mainstream channel are 15 m/s, and 3.5%, respectively. The static pressure at the outlet of mainstream channel is set as atmospheric pressure. The Reynolds number based on velocity at the inlet of mainstream channel and cooling hole diameter is 5587. The turbulence intensity of the coolant flow at the inlet of the plenum chamber is 1.0%. In order to keep the coolant-to-mainstream density ratio DR of 1.38 the same as that in [16], the temperatures at the

Fig. 1 Sketch of computational model. **a** overview. **b** details of crescent-shaped block. **c** streamwise positions of crescent-shaped block

(a) overview

(b) details of crescent-shaped block

(c) streamwise positions of crescent-shaped block
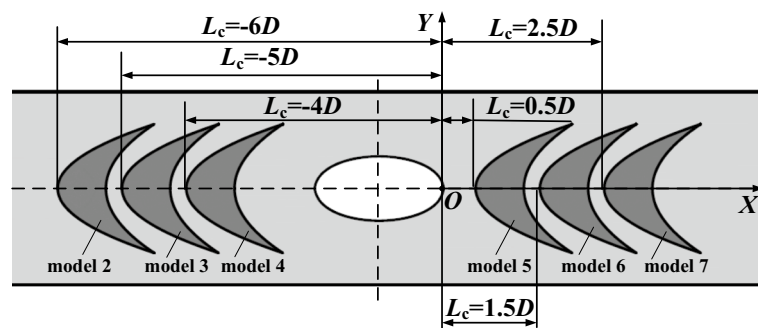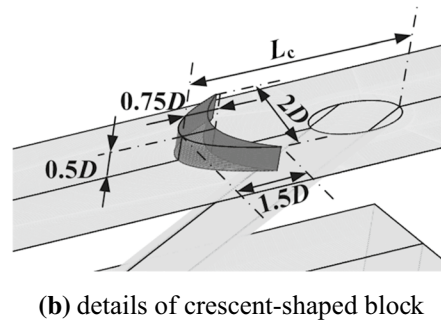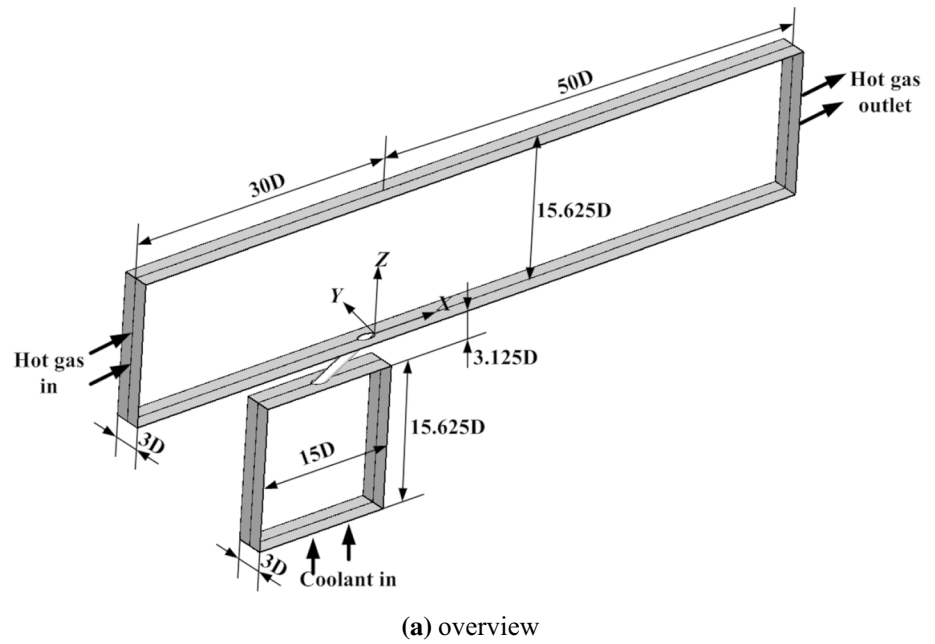
inlet of mainstream channel T_m and at the inlet of plenum chamber T_c are set with the values of 414 K and 300 K, respectively. The coolant flow at the inlet of plenum chamber is perpendicular to the flow direction in the mainstream channel. The velocities at the inlet of plenum chamber are calculated, respectively, to obtain the three blowing ratios M with values of 0.5, 1.0 and 1.5.

The blowing ratio M can be defined as follow

$$M = \mathrm{DR} \cdot \frac{U_c}{U_m} \tag{1}$$

where U_c is the averaged velocity at the inlet of the cooling hole.

Planes $Y/D = -1.5$ and $Y/D = 1.5$ are both set as periodic conditions to model the row of cooling holes with infinite numbers. All the walls of the mainstream channel, cooling

hole, plenum chamber and crescent-shaped block are set to be adiabatic with no-slip conditions.

2.4 Data reduction

Cooling effectiveness η and non-dimensional temperature θ are defined as, respectively

$$\eta = \frac{T_{aw} - T_m}{T_c - T_m} \tag{2}$$

$$\theta = \frac{T_c - T_f}{T_c - T_m} \tag{3}$$

where T_{aw} is the adiabatic temperature over the bottom wall of the mainstream channel, and T_f is the temperature of the mixture of mainstream hot gas and coolant.

The laterally averaged cooling effectiveness $\bar{\eta}$ over the pitch of $3D$ and the area-averaged cooling effectiveness $\bar{\bar{\eta}}$ in the region ($0 \leq X/D \leq 30$, $-1.5 \leq Y/D \leq 1.5$) are calculated as, respectively

$$\bar{\eta} = \frac{1}{3D} \int_{-1.5D}^{1.5D} \eta \, dY \tag{4}$$

$$\bar{\bar{\eta}} = \frac{1}{1.5D \times 28D} \int_{2D}^{30D} \int_{0}^{1.5D} \eta \, dY dX \tag{5}$$

Vorticity in X direction ω_X, i.e., the streamwise vorticity, is calculated to illustrate the intensity of the CRVP, which is defined as

$$\omega_X = \frac{\partial U_Z}{\partial Y} - \frac{\partial U_Y}{\partial Z} \tag{6}$$

where U_Y and U_Z are the velocities in Y direction and Z direction, respectively.

The mixing losses caused by the film cooling can be divided into aerodynamic loss and aerothermal loss, as described in [22, 23]. Although the entropy generation is not considered for the mixing of the mainstream flow and the coolant flow, the aerodynamic loss is customarily used as an evaluation criterion, which is also the selection in present study. Traditionally, the total pressure loss coefficient is used to indicate the aerodynamic loss. Assuming the mainstream flow and the coolant flow is mixed ideally, the total pressure of the mixing flow $p_{t,mix}$ can be calculated as follow [22]

$$p_{t,mix} = \frac{m_c}{m_c + m_m} p_{t,cin} + \frac{m_m}{m_c + m_m} p_{t,m} \tag{7}$$

where m_c and m_m are the mass flow rates of the coolant and the mainstream hot gas, respectively, $p_{t,cin}$ and $p_{t,m}$ are the total pressure at the inlet of cooling hole and at the inlet of mainstream channel, respectively.

Thus, the total pressure loss coefficient can be calculated based on the total pressure of the mixing flow, which is expressed as follow

$$\xi = \frac{p_{t,mix} - p_{t,f}}{\rho_m U_m^2 / 2} \tag{8}$$

where $p_{t,f}$ is the total pressure at the outlet of mainstream channel and ρ_m is the density of the mainstream hot gas at the inlet of the mainstream channel.

2.5 Grid sensitivity

The grids for models 1–7 are all generated as structured meshes by using the software package ANSYS ICEM CFD. Figure 2 shows the grids for model 3 with upstream block ($L_c = -5D$) and for model 5 with downstream block ($L_c = 0.5D$) around the hole. The grids are refined near the walls of mainstream channel, cooling hole, plenum chamber and the block. The grids in the near-wall layers are stretched away from the walls with a growth ratio of 1.2.

Based on the requirement of the k–ω SST turbulence model, the value of y^+ is carefully checked to keep in the
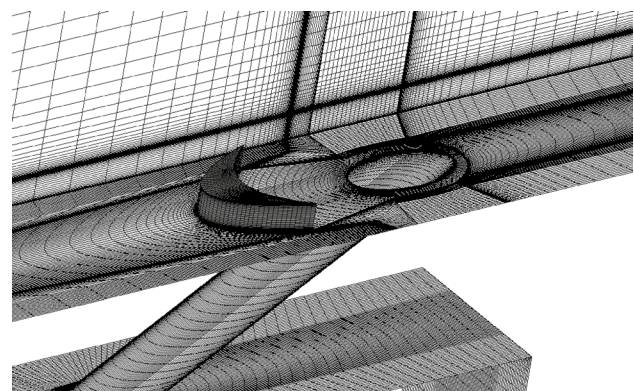
(a) model 3 with upstream block
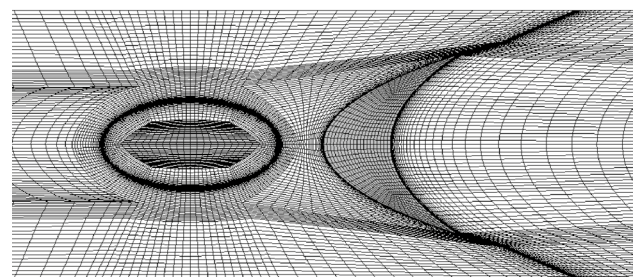
(b) model 5 around the hole

Fig. 2 Computational grids. **a** model 3 with upstream block. **b** model 5 around the hole

order of unity or less. The calculation formula of y^+ is shown as follow

$$y^+ = \frac{u_* \cdot y}{\nu} \qquad (9)$$

where u_* is the friction velocity at the nearest wall, y is the distance between the first and second mesh points off the wall, ν is the local kinematic viscosity of the fluid. The values of y^+ along all walls can be viewed in the CFX Post.

The grid sensitivity tests are carried out to confirm that the simulation results are independent with the grid numbers. The non-dimensional temperature profile along the intersection line of plane $X/D = 5$ and plane $Y/D = 0$ is selected to be the criterion. Figure 3 shows the calculated results for model 1 at $M = 0.5$ with three grid levels. The numbers of grids investigated are 1.61 million, 2.06 million and 2.62 million, respectively. It can be seen that when the grid number reaches to 2.06 million, the influence of grids with further increased numbers can be ignored. So the grid with 2.06 million cells is adopted in all the following simulations for model 1. Grid sensitivity tests are also performed for models 2–7 in similar methods. The numbers of independent grids for models 2–7 are ranged from 3.08 million to 3.53 million according to the streamwise position of the block.

2.6 Validation study

Two typical calculated cases for model 1 without block at $M = 0.5$ and the configuration with downstream block at $M = 1.0$ are selected to validate current calculated results. The calculated results with the k-ω SST turbulence model are compared with the experimental data in [16, 24] in similar geometries and operating conditions, which are shown in Fig. 4. It is worthy noting that the geometries and the operating conditions for calculations are the same with ones in [16]
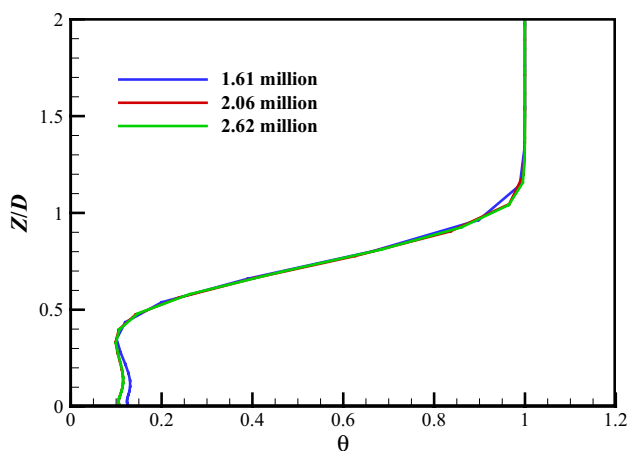

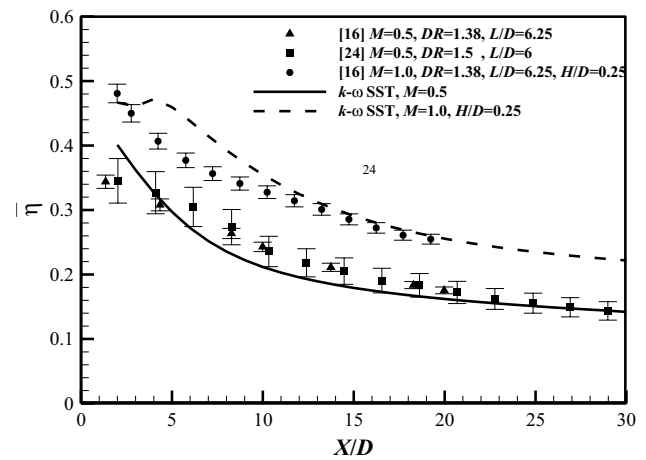**Fig. 3** Grid sensitivity test for model 1

Fig. 4 Comparison between calculated results and experimental data

($L/D = 6.25$, $DR = 1.38$, $H/D = 0.25$), but slightly different with the ones in [24] ($L/D = 6$, $DR = 1.5$). The uncertainties of experimental data in [16] [24] are 3% and 7%, respectively. It can be seen that the calculated results can correctly depict the change trend of the laterally averaged cooling effectiveness along the streamwise direction. Although the calculated laterally averaged cooling effectiveness is underestimated in the middle downstream region of the hole at $M = 0.5$ and over-predicted in the near downstream region of the block at $M = 1.0$, the overall prediction is in reasonable agreement. Alternative approaches with more accuracy in ANSYS CFX such as LES or Detached Eddy Simulation (DES) are not considered in present study, because they are computationally expensive and not suitable for practical industrial computations. Therefore, the RANS approach with k–ω SST turbulence model is adopted in all the following calculations.

3 Results and discussions

3.1 Flow field

Figure 5 shows the surface streamlines and non-dimensional temperature contours on plane $Y/D = 0$ at $M = 1.0$. For model 1 without block, ejected coolants penetrate into the mainstream flow and are lifted away from the wall because of their large enough momentum. For models 2–4 with upstream blocks, the approaching boundary layer ahead of the hole is disturbed by the obstruction of the block. The mainstream hot gas firstly flows over the tip of the block, and then impinges on the ejected coolants just away the hole. So the penetration height into the mainstream flow decreases, and the ejected coolants are suppressed by the deflected mainstream flow and reattached to the wall downstream the
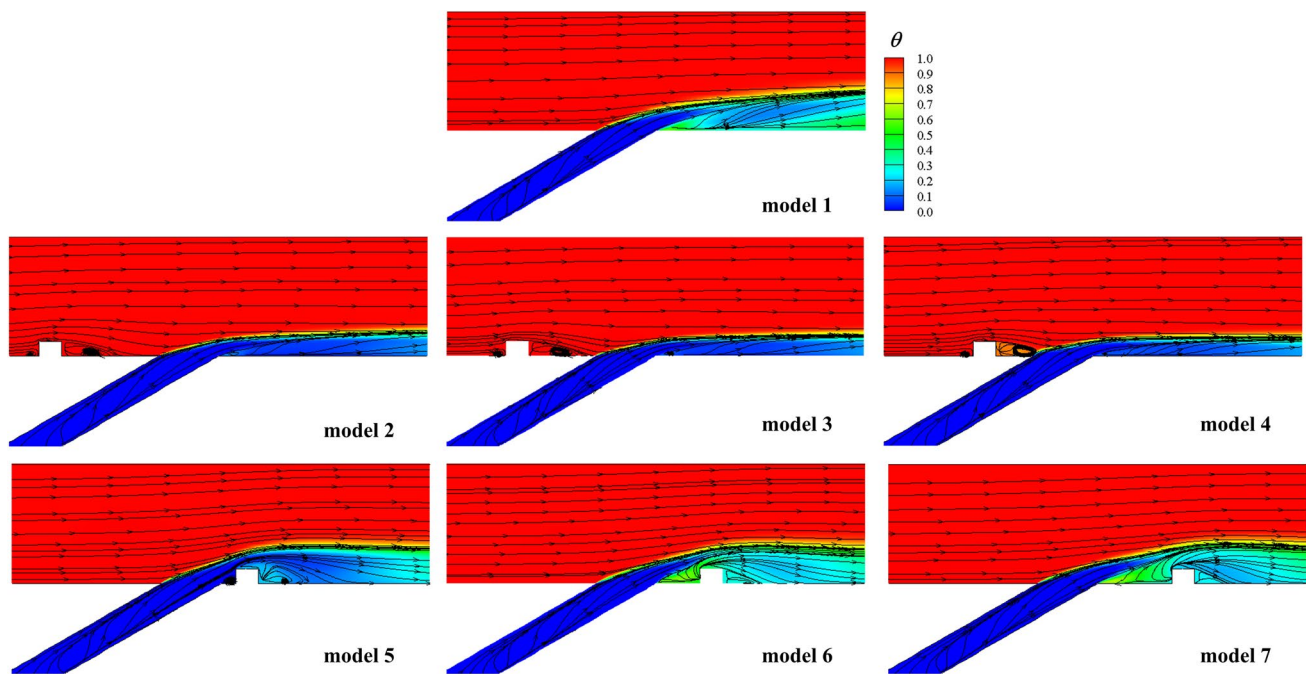
Fig. 5 Streamlines and contours of non-dimensional temperature on plane $Y/D = 0$ at $M = 1.0$

hole. Due to the backward-facing step effect induced by the upstream block, the separation flow grows just behind the trailing edge of the block. With the decrease in the absolute streamwise distance L_c for models 2–4, the growing scale of the separation flow is gradually decreased. For the model 4 with the shortest distance ($L_c = -4D$), the separation flow grows insufficiently. Hence, a few of coolants are extracted reversely to the region between the block and the hole for model 4. When the block is placed downstream the hole for models 5–7, the boundary layer downstream the hole for the coolant flow is altered directly and violently. Part of ejected coolants flow over the block tip and then bends downward to the wall. Another part of coolants is lifted away higher from the wall due to the occupation by the block. As the downstream block is laid back gradually, the amount of the blocked coolants is consequently decreased from model 5 ($L_c = 0.5D$) to model 7 ($L_c = 2.5D$). Meanwhile, the penetration heights into the mainstream flow for models 5–7 are comparatively equal to that for model 1.

Figure 6 shows the 3D streamlines of the coolants ejected from the hole and the mainstream hot airs from the upstream plane with vertical range of $0 \leq Z/D \leq 0.75$ for models 1–7 at $M = 1.0$. The streamlines in Fig. 6 are all colored with non-dimensional temperature θ in order to better illustrate the flows of coolants and mainstream hot airs. It can be seen that the ejected coolants and the mainstream hot airs occupy the middle region and the sideways in lateral direction, respectively, for model 1. For models 2–4 with upstream blocks, twisted flows are generated by the interaction between the

upstream block and mainstream hot airs. Part of ejected coolants is entrained to the sideways in lateral direction by the twisted hot air flows and further flows downstream along the streamwise direction. As the upstream block is placed nearer the hole, the sweeping flow past over the tip of the block gradually strikes directly on the ejected coolants just from the hole. Most of the ejected coolants still locates at the middle region for models 2–4 with upstream block. For models 5–7 with downstream block, ejected coolants are obstructed and dissipated by the downstream block. Twisted flows are also generated just downstream the block yet by the interaction between the ejected coolants and the block. The twisted coolant flows occupy most of the region in lateral direction, and push the coolants to sideways. As the downstream block is placed further the hole, the twisted flows are generated at further streamwise position, and the unaffected region becomes wider.

In order to better illustrate the influence of block on the original CRVP, both surface streamlines and contours of streamwise vortex ω_X on planes $X/D = 5$ and 10 for models 1–7 at $M = 1.0$ are shown in Fig. 7. It can be clearly seen that the CRVP dominates the flow fields downstream the hole on planes $X/D = 5$ and 10 for model 1 without block. The CRVP lifts the ejected coolants off the wall and ventilates the mainstream hot airs toward the center position in the lateral direction. The development of CRVP shows the decrease in vortex intensity from plane $X/D = 5$ to plane $X/D = 10$ with the mixing between the coolants and the mainstream hot airs. For model 2 with upstream block, the
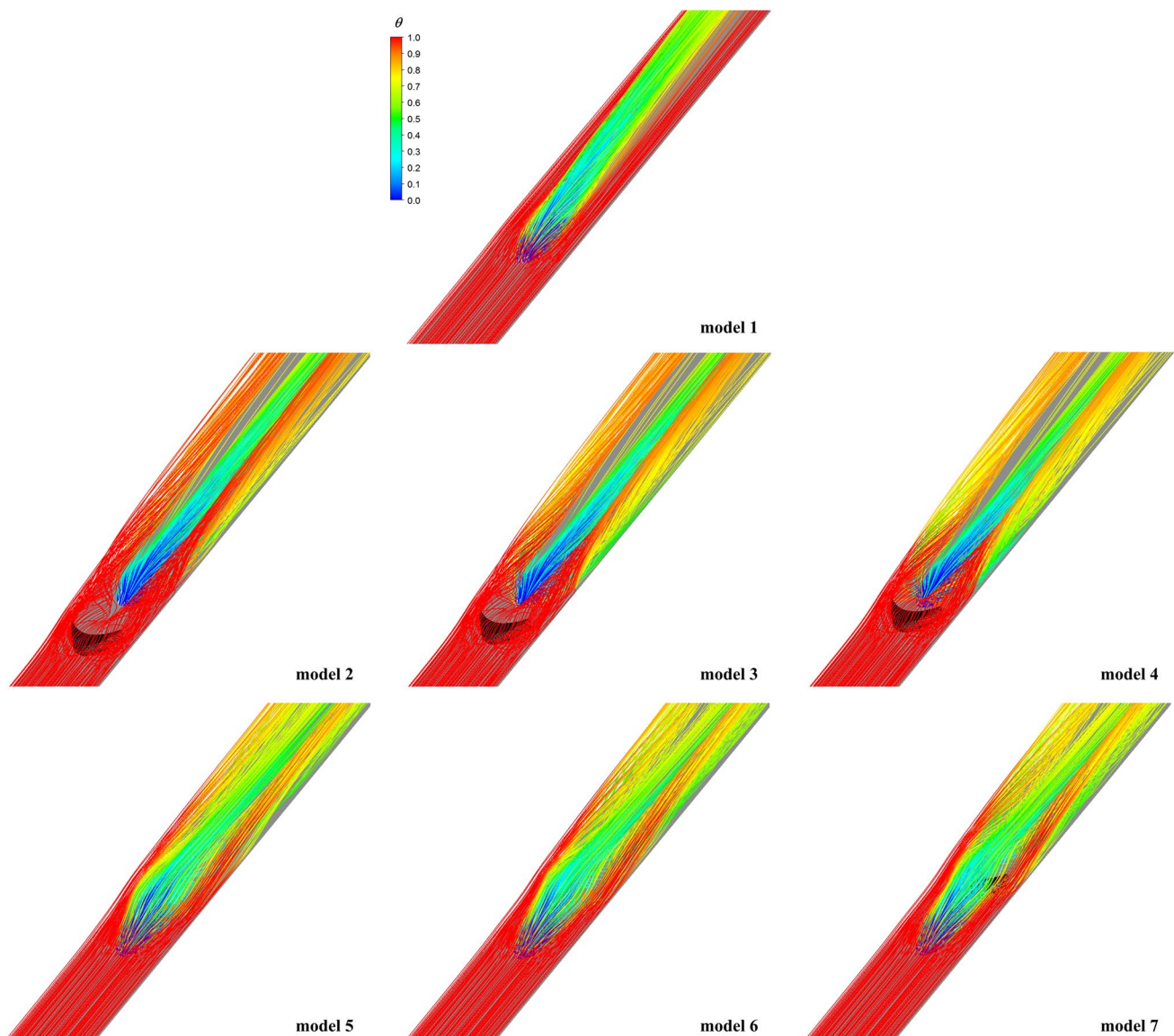
Fig. 6 3D streamlines around the hole and the block at $M = 1.0$

twisted hot air flows induced by the upstream block in Fig. 6 illustrate additional vortex pair on planes $X/D = 5$ and 10. The additional pair of vortex rotates in the opposite direction with the original CRVP, which is named anti-CRVP in present study. The anti-CRVP locates at the sideways in the lateral direction. With the presence of the anti-CRVP, the CRVP shows the decrease in the scale and intensity with a large margin and is suppressed to stay closer to the wall. As a result, transverse hot air flows induce lateral ventilation dragging the coolants at the middle section to sideways. In comparison with the vortex intensities on plane $X/D = 5$ and $X/D = 10$ for model 1, the intensity of CRVP for model 2 decreases dramatically due to the energy input from the anti-CRVP. When the upstream block is placed closer to the hole for models 3 and 4, the intensity becomes stronger.

Thus, the suppression effect on the CRVP is more violent, which results in the CRVP with smaller scale and weaker intensity especially on plane $X/D = 10$ in comparison with model 2. It is worthy noting that the upstream block hinders the development of CRVP, but cannot eliminate the generation of CRVP. For models 5–7 with downstream block, the twisted coolant flows induced by the downstream block also generate an additional anti-CRVP on planes $X/D = 5$ and 10. As compared with the vortex structures for models 2–4 with upstream block, the CRVP is lifted away from the wall and is weaken dramatically even almost disappear on plane $X/D = 10$. One reason is that the coolant core bleeding from the hole is broken and diffused greatly by the obstruction of the block. The other important reason is that the anti-CRVP is strong enough to eliminate the CRVP with
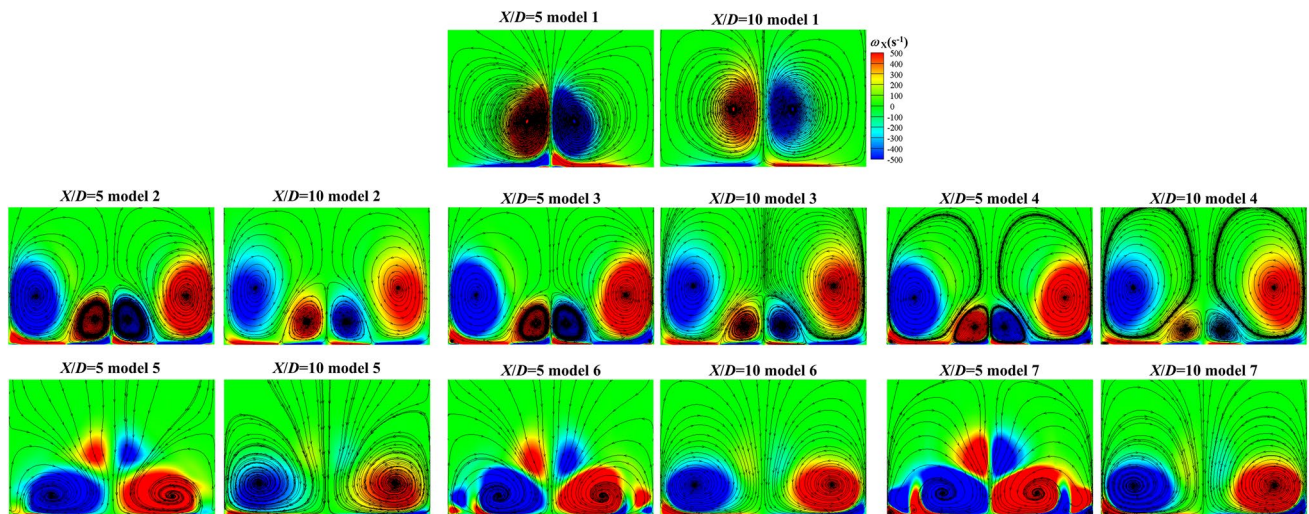
Fig. 7 Streamlines and contours of streamwise vorticity on planes $X/D = 5$ and 10 at $M = 1.0$

the direct influence of downstream block on ejected coolants. But as the block is placed further away from the hole, the CRVP becomes more and more obvious from model 5 ($L_c = 0.5D$) to model 7 ($L_c = 2.5D$). This is mainly caused by the decrease in the blockage effect from the downstream block. The anti-CRVP for models 5–7 stays closer to the wall than the ones for models 2–4 with upstream blocks and covers the whole region in the pitch.

3.2 Coolant coverage and cooling effectiveness

The contours of cooling effectiveness over the wall for models 1–7 are illustrated in Fig. 8 at $M = 1.0$. It is quite clear that the application of a block whether upstream or downstream the hole achieves considerable expansion of coolant coverage in lateral direction with higher cooling effectiveness than model 1. The ejected coolants cover almost

the whole pitch region after streamwise location $X/D = 3$ for model 2, $X/D = 1$ for model 3, $X/D = 0$ for model 4 and $X/D = 6$ for models 5–7, respectively. Because the ejected coolants are suppressed to be stayed closer to the wall and ventilated toward the sideways by the anti-CRVP in Fig. 7, the area of high cooling effectiveness region ($\eta > 0.3$) increases greatly for models 2–4. But two regions with lower cooling effectiveness exist at the far downstream position, which correspond to the regions not covered by the streamlines of coolant flows in Fig. 6. In comparison with model 2, as the absolute distance between the block and the hole decreases, the region between the block and the hole exhibits better coolant coverage for models 3 and 4 due to more coolants entrained by the incomplete fully developed backflow shown in Fig. 5. For model 5 with downstream block, cooling effectiveness is higher over the region between the hole and the block, since some coolants are obstructed by the
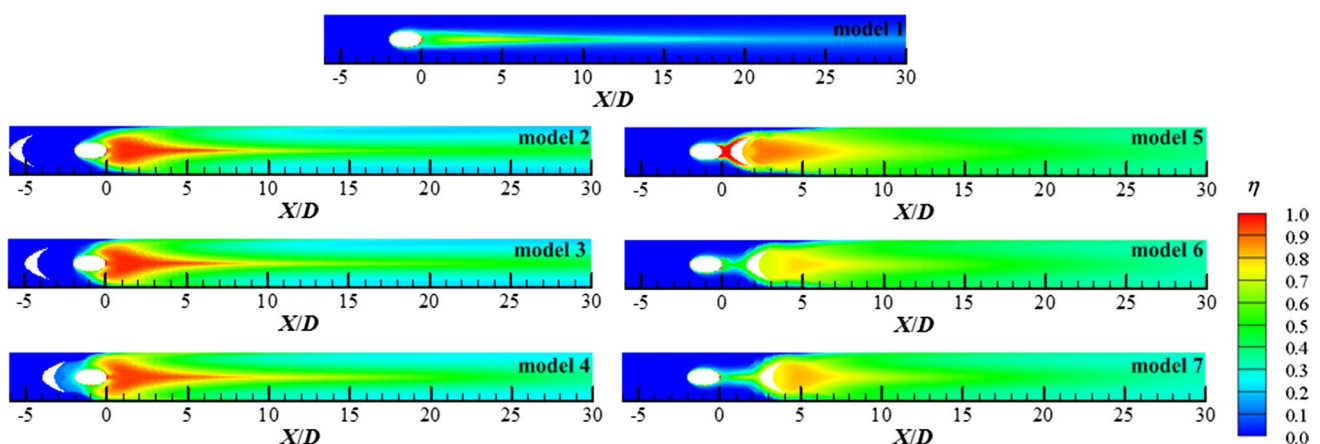

Fig. 8 Contours of cooling effectiveness over the wall at $M = 1.0$

block and collected over this region. Because the blocked coolants are attached to the wall by the anti-CRVP, most of the regions downstream the block exhibit high cooling effectiveness ($\eta > 0.3$). As the block is placed further downstream away from the hole, the cooling effectiveness distributions between the hole and the block for models 6–7 are somewhat like that for model 1 because of the decreasing in the obstruction effect. Comparatively, the downstream block results in more uniform coolant coverage and cooling effectiveness over the downstream region after streamwise location $X/D = 6$.

The contours of cooling effectiveness for models 1–7 at lower blowing ratio $M = 0.5$ (seen in Fig. 9) and higher blowing ratio $M = 1.5$ (seen in Fig. 10) will be illustrated and compared with the one at medium blowing ratio $M = 1.0$ to investigate the effect of blowing ratio.

As compared with Fig. 8 at $M = 1.0$, the coolant coverage at $M = 0.5$ in Fig. 9 is improved over the whole region for model 1 without block, but worse for models 2–7 with block

especially over the latter region downstream the hole. Since the coolants eject from the hole with lower momentum flux at $M = 0.5$, the strengths of the CRVP and the anti-CRVP are both weaker. For model 1 without block, the ejected coolants are attached to the wall due to their lower momentum flux, but in poor lateral spreading by the detrimental effect of the CRVP. The upstream blocks for models 2–4 improve the coolant coverage over the front region downstream the hole by the help of the anti-CRVP with weaker intensity. Although the coolants are still attached to the wall for models 2–4, the amount of coolants flowing downwards decreases due to some of coolants are dragged to sideways. Therefore, the cooling effectiveness dramatically decreases along the streamwise direction and the coolant coverage degrades over the latter region downstream the hole. For model 4 with block closest to the hole, the area with better coolant coverage and higher cooling effectiveness decrease compared with the ones for model 2. Similar as model 4 at $M = 1.0$ in Fig. 8, the region between the block and the
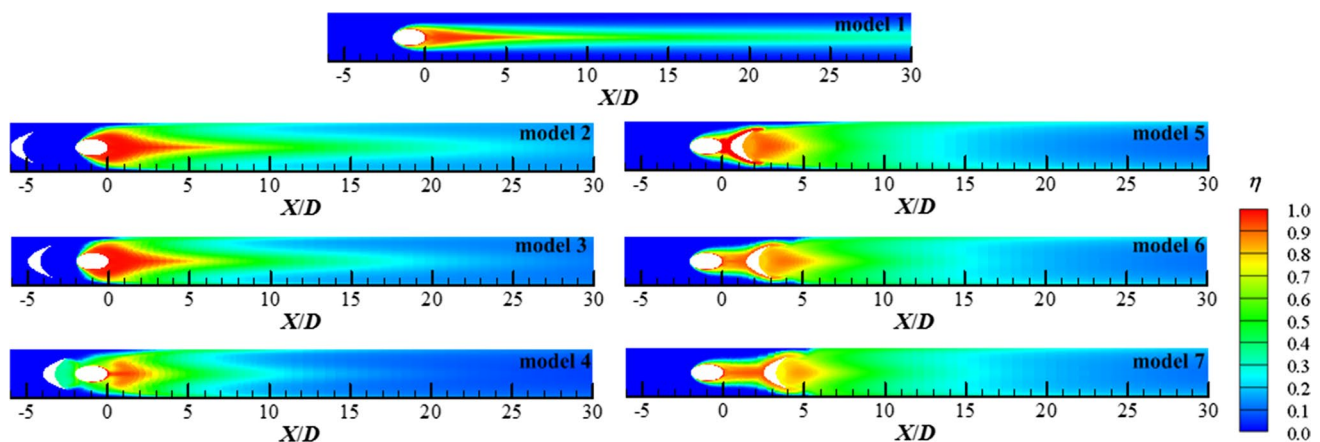

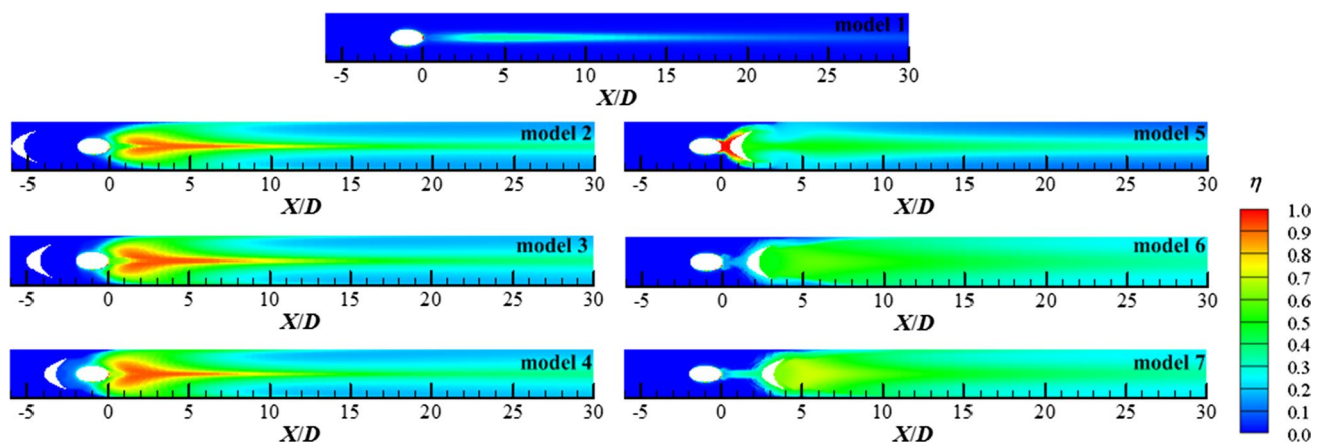**Fig. 9** Contours of cooling effectiveness over the wall at $M = 0.5$

Fig. 10 Contours of cooling effectiveness over the wall at $M = 1.5$

hole is covered with more coolants for model 4 at a lower blowing ratio $M = 0.5$. For models 5–7 with downstream block at $M = 0.5$, most of the ejected coolants are blocked and flow along the windward side to sideways due to the lower penetration height into the mainstream channel. This results in relatively higher cooling effectiveness at sideways. Besides, the cooling effectiveness for models 5–7 decreases nearby the centerline over the region after the reattached flow induced by the backward-facing strep effect. Comparatively, the regions downstream the block with higher cooling effectiveness are almost the same for models 5–7.

Compared with the effectiveness distributions over the wall at $M = 1.0$ in Fig. 8, the models 1–7 at a higher blowing ratio $M = 1.5$ show worse coolant coverage, which can be seen in Fig. 10. With the increasing of blowing ratio from 1.0 to 1.5, the coolants are lifted off away the wall higher and thus poorer coolant coverage with lower cooling effectiveness achieves for model 1 without block. The distributions of coolant coverage for models 2–4 at $M = 1.5$ are almost similar as the ones at $M = 1.0$. The strengths of the detrimental CRVP increase for models 2–4 at $M = 1.5$; thus, the suppression effects of the anti-CRVP decrease, which cause the decrease in the cooling effectiveness as the ones at $M = 1.0$. The distribution patterns for models 6–7 with downstream blocks at $M = 1.5$ are also almost similar as the ones with the ones at $M = 1.0$. But model 4 at $M = 1.5$ exhibits a quite different distribution of cooling effectiveness from model 4 at $M = 1.0$. Due to the higher penetration into the mainstream flow at $M = 1.5$, the amount of coolants blocked by the downstream block decreases; thus, the effect of the anti-CRVP degrades. Therefore, the coolant coverage is worse over the whole region especially at the sideways. Besides, the distribution of cooling effectiveness for model 4 at $M = 1.5$ shows a clear reattachment of coolants downstream the block.

In order to investigate the possibility of reduction in coolant consumption, area-averaged cooling effectiveness is calculated for models 1–7 at blowing ratios $M = 0.5$, 1.0 and 1.5 and compared in Fig. 11. Note that model 1 is denoted with $L_c = 0$ in convenience in spite of no practical physical meaning. The hole exit is also illustrated in Fig. 11. It is obviously clear that the block placed whether upstream (models 2–4) or downstream (models 5–7) always has positive influence on the improvement of area-averaged cooling effectiveness at all three blowing ratios. But the area-averaged cooling effectiveness differs each other for configurations with block located at various streamwise positions and at different blowing ratios. At $M = 0.5$, the area-averaged cooling effectiveness for models 2–4 monotonously decreases as the upstream block moves closer to the hole. The value of area-averaged cooling effectiveness at $M = 0.5$ decreases from 0.336 for model 2 to 0.221 for model 4. But models 5–7 with downstream block yield the area-averaged cooling
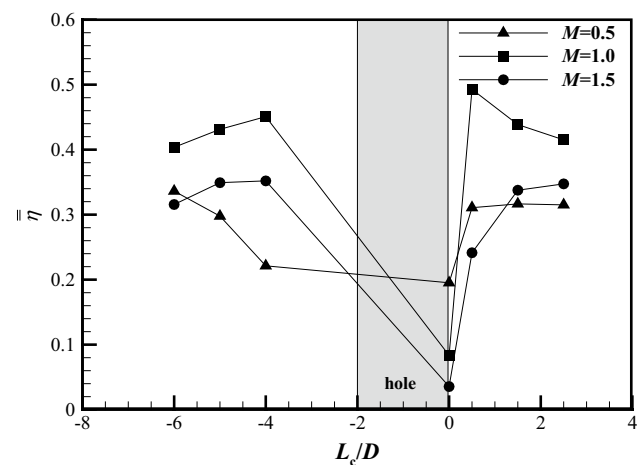

Fig. 11 Area-averaged cooling effectiveness at blowing ratios $M = 0.5$, 1.0 and 1.5

effectiveness ranged from 0.310 to 0.316, which show a narrow variation range as compared with models 2–4. At $M = 1.0$ and 1.5, the area-averaged cooling effectiveness monotonously increases for models 2–4 with the decrease in the absolute streamwise distance. For models 5–7 with downstream block, as the streamwise distance increases, the area-averaged cooling effectiveness decreases from 0.493 for model 5 to 0.415 for model 7 at $M = 1.0$ but increases from 0.241 for model 5 to 0.347 for model 7. The maximum area-averaged cooling effectiveness can be obtained with the value of 0.336 for model 2 at $M = 0.5$, 0.493 for model 5 at $M = 1.0$ and 0.352 for model 4 at $M = 1.5$, respectively. Comparatively, the area-averaged cooling effectiveness at $M = 1.0$ for all models outperforms for the corresponding model at the other two blowing ratios, which is in accordance with the contours of cooling effectiveness over the wall with higher values in Fig. 8. From the above analysis, we can conclude that the specific area-averaged cooling effectiveness varies based on the blowing ratio and the streamwise position of the block. Of particularly, model 5 ($L_c = 0.5D$) at blowing ratio $M = 1.0$ has the best area-averaged cooling effectiveness.

3.3 Aerodynamic loss

Aerodynamic loss is another important parameter to evaluate the film cooling performance. Figure 12 shows the aerodynamic losses for models 1–7 at blowing ratios $M = 0.5$, 1.0 and 1.5. It can be seen that the aerodynamic losses always increase by placing the block upstream or downstream the hole as compared with model 1. As the separation flow induced by the upstream block grows insufficiently for model 4 ($L_c = -4D$), the aerodynamic loss is lower than those for other models with upstream block at the same blowing ratio.
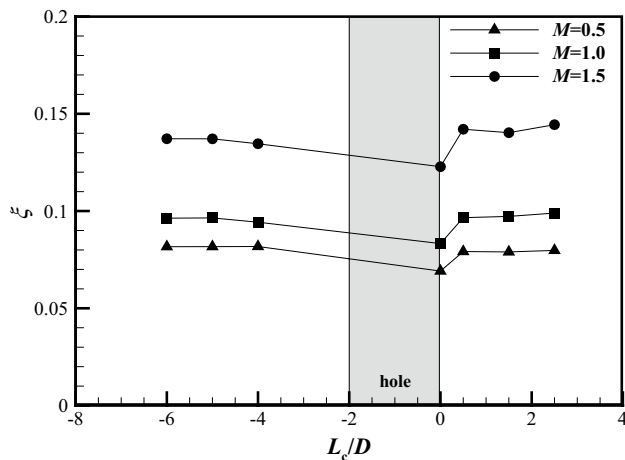
Fig. 12 Aerodynamic loss at blowing ratios $M = 0.5$, 1.0 and 1.5

Fig. 13 Comprehensive evaluations for models 1–7 (symbols: triangular—$M = 0.5$; square—$M = 1.0$; circle—$M = 1.5$)

Models 2–3 have comparative aerodynamic loss at either blowing ratio because of the sufficient developing separation flow after the block. As compared with models 2–4, models 5–7 with downstream block yield a bit lower aerodynamic losses at $M = 0.5$. But as the blowing ratio increases, the aerodynamic losses for models 4–7 are higher than those for models 2–4. Moreover, it can be seen that the aerodynamic losses increase with the increase in blowing ratio for each model.

3.4 Comprehensive evaluation

Taken the area-averaged cooling effectiveness and aerodynamic loss for model 1 at $M = 0.5$ as the evaluation basic, the relative area-averaged cooling effectiveness η_{rel} and relative aerodynamic loss ξ_{rel} can be calculated, respectively. Taking above-mentioned two performance parameters into account, η_{rel} and ξ_{rel} for models 1–7 at blowing ratios $M = 0.5$, 1.0 and 1.5 are shown in Fig. 13 and their values are listed in Table 1 at the meantime. It can be seen that variation region of ξ_{rel} for models 2–7 is narrower than that of η_{rel} at either blowing ratio. For example, the variation region at $M = 1.0$ is 0.456 for η_{rel}, but only 0.068 for ξ_{rel}. Hence, the effect of the streamwise position is weaker on the aerodynamic loss than on the area-averaged cooling effectiveness. It can be easily seen that all models with block neither upstream or downstream exhibit lower in terms of the relative area-averaged cooling effectiveness at $M = 0.5$ and 1.5, but higher at $M = 1.0$. Besides, models 2–7 showed incremental relative aerodynamic loss as the blowing ratio increases from $M = 0.5$ to $M = 1.5$. For a specific film cooling design, higher area-averaged cooling and lower aerodynamic loss are usually preferred. Following this evaluation criterion, we can easily point out model 4 is the optimal design due to its highest η_{rel} and lowest ξ_{rel} in all models investigated in present
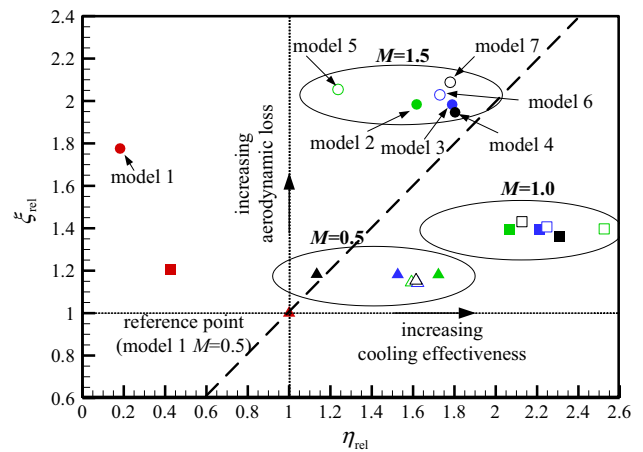
study when the working condition is $M = 1.5$. But when the blowing ratios equal to be 0.5, model 2 gives highest relative area-averaged cooling effectiveness but medium relative aerodynamic loss. The same situation occurs for model 5 at $M = 1.0$ as that at $M = 0.5$. Hence, the superiority of the model at $M = 0.5$ and 1.0 cannot be evaluated explicitly.

According to the authors' knowledge, there has been no clear comprehensive evaluation proposed up to now in the consideration of both cooling effectiveness and aerodynamic loss. In present study, a new criterion η_{comp} is defined to evaluate the film cooling comprehensive performance accounting for cooling effectiveness and aerodynamic loss, which can be calculated as follow

$$\eta_{comp} = \frac{\eta_{rel}}{\xi_{rel}} \tag{10}$$

If η_{comp} has a higher value, this means that that the model has higher cooling performance and lower aerodynamic loss, and thus better film cooling comprehensive performance. This parameter can be clearly evaluated the comprehensive performance for different models at the same blowing ratio.

Figure 14 shows the film cooling comprehensive evaluations for models 1–7 at $M = 0.5$, 1.0 and 1.5, respectively. At $M = 1.5$, model 4 has highest comprehensive performance with the value of 0.926. Hence, $Lc = -4D$ is the optimal streamwise position at $M = 1.5$. This conclusion is in accordance with the analysis on the criterion of area-averaged cooling effectiveness in Fig. 13 at $M = 1.5$. At $M = 0.5$, the comprehensive performance with the value of 1.458 is achieved for model 2, which is slightly higher than those for model 3 and models 5–7. But, model 4 shows almost comparative comprehensive performance with model 1 without block at $M = 0.5$. At $M = 1.0$, models 2–7 show remarkable improvements on the basic of model 1, and model 5 exhibits highest comprehensive performance with value of 1.807. It can be

Table 1 Summary of the relative area-averaged cooling effectiveness and aerodynamic loss for models 1–7

	M = 0.5		M = 1.0		M = 1.5	
	η_{rel}	ξ_{rel}	η_{rel}	ξ_{rel}	η_{rel}	ξ_{rel}
Model 1	1.000	1.000	0.428	1.204	0.182	1.776
Model 2	1.723	1.181	2.068	1.393	1.617	1.984
Model 3	1.526	1.182	2.210	1.395	1.789	1.983
Model 4	1.134	1.183	2.310	1.363	1.803	1.947
Model 5	1.592	1.145	2.525	1.397	1.237	2.054
Model 6	1.622	1.142	2.247	1.407	1.730	2.029
Model 7	1.614	1.154	2.127	1.431	1.780	2.088
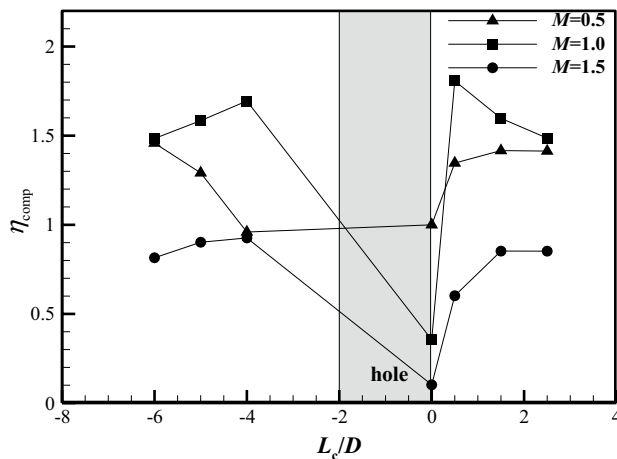
Fig. 14 Comprehensive evaluations for models 1–7

found that the optimal models obtained in terms of the comprehensive performance are exactly the same as the ones in terms of area-averaged cooling effectiveness. This is mainly caused by the narrow variation of the relative aerodynamic loss, which can be clearly seen in Fig. 12.

4 Conclusions

In this study, the effect of streamwise position of crescent-shaped block of a row of circular holes on flow field, cooling effectiveness and aerodynamic loss at three blowing ratios $M = 0.5$, 1.0 and 1.5 are systematically investigated by using the numerical method. Totally seven models including model 1 without block, models 2–4 with upstream blocks ($L_c = -6D$, $-5D$ and $-4D$) and model 5–7 with downstream block ($L_c = 0.5D$, $1.5D$ and $2.5D$) are simulated. The downstream vortex structures, cooling effectiveness and aerodynamic loss are analyzed in details. The following conclusions can be summarized as follows:

(1) Compared with model 1 without block, the flow property of the ejected coolant is altered by the crescent-shaped block placed whether upstream or downstream the hole, and the detrimental effect of the CRVP is weakened by the additional anti-CRVP. When the block is located upstream the hole, the interaction between the mainstream hot airs and the block results in the generation of the anti-CRVP, which suppresses the coolants to be attached on the wall and improves the coolant coverage in the lateral direction. But if the block is placed downstream the hole, the anti-CRVP is induced by the interaction between the ejected coolants and the block, which can also expand the lateral coolant coverage.

(2) The upstream or downstream block improves the area-averaged cooling effectiveness at blowing ratios ranged from 0.5 to 1.5. But the area-averaged cooling effectiveness varies for configurations with block at different streamwise positions and at various blowing ratios. The maximum area-averaged cooling effectiveness achieves for model 2 at $M = 0.5$, for model 5 at $M = 1.0$, but for model 4 at $M = 1.5$.

(3) The aerodynamic losses for models with the presence of block whether upstream or downstream are higher than the model without block. The aerodynamic losses increase for either model with the increasing of blowing ratio. Comparatively, models 5–7 with downstream block have slight lower aerodynamic losses than models 2–4 with upstream block at $M = 0.5$, but higher aerodynamic losses at $M = 1.0$ and 1.5.

(4) A new comprehensive criterion for film cooling is proposed in consideration of both cooling performance and aerodynamic loss. Due to the narrow variation of the aerodynamic loss for the models investigated in present study, the configurations with highest comprehensive performance are still model 4 at $M = 0.5$, model 5 at $M = 1.0$ and model 4 at $M = 1.5$, respectively.

Compliance with ethical standards

Conflict of interest The authors declare that there is no conflict of interests regarding the publication of this paper.

References

1. Fric TF, Roshko A (1994) Vortical structure in the wake of a transverse jet. J Fluid Mech 279:1–47

2. An BT, Liu JJ, Zhang XD, Zhou SJ, Zhang C (2016) Film cooling effectiveness measurements of a near surface streamwise diffusion hole. Int J Heat Mass Transf 103:1–13

3. Bunker RS (2005) A review of shaped hole turbine film-cooling technology. ASME J Heat Transfer 127:441–453

4. Kusterer K, Bohn D, Sugimoto T, Tanaka R (2007) Double-jet ejection of cooling air for improved film cooling. ASME J Turbomach 129:809–815

5. Heidmann JD, Ekkad S (2008) A novel antivortex turbine film-cooling hole concept. ASME J Turbomach 130:031020

6. Nasir H, Acharya S, Ekkad S (2003) Improved film cooling from cylindrical angled holes with triangular tabs: effect of tab orientations. Int J Heat Fluid Flow 24:657–668

7. Na S, Shih TI-P (2007) Increasing adiabatic film-cooling effectiveness by using an upstream ramp. ASME J Heat Transf 129:464–471

8. Zheng DR, Wang XJ, Zhang F, Yuan Q (2017) Numerical investigation on the effects of the divided steps on film cooling performance. Appl Therm Eng 124:652–662

9. Kawabata H, Funazaki K, Nakata R, Takahashi D (2014) Experimental and numerical investigations of effects of flow control devices upon flat-plate film cooling performance. ASME J Turbomach 136:061021

10. Kawabata H, Funazaki K, Suzuki Y, Tagawa H, Horiuchi Y (2016) Improvement of turbine vane film cooling performance by double flow-control devices. ASME J Turbomach 138:111005

11. Sarkar S, Ranakoti G (2017) Effect of vortex generators on film cooling effectiveness. ASME J Turbomach 139:061009

12. Zhou WW, Hu H (2017) A novel sand-dune-inspired design for improved film cooling performance. Int J Heat Mass Transf 110:908–920

13. Zaman KBMQ, Rigby DL, Heidmann JD (2010) Inclined jet in crossflow interacting with a vortex generator. AIAA J Propuls Power 26:947–954

14. Shinn AF, Vanka SP (2013) Large eddy simulations of film-cooling flows with a micro-ramp vortex generator. ASME J Turbomach 135:011004

15. Song LM, Zhang C, Song YJ, Li J, Feng ZP (2017) Experimental investigations on the effects of inclination angle and blowing ratio on the flat-plate film cooling enhancement using the vortex generator downstream. Appl Therm Eng 119:573–584

16. An BT, Liu JJ, Zhang C, Zhou SJ (2013) Film cooling of cylindrical hole with downstream short crescent-shaped block. ASME J Heat Transf 135:031702

17. Khoris A, Guelailia A, Hamidou MK (2016) Improvement of film cooling effectiveness with a small downstream block body. J Appl Mech Tech Phy 57:666–671

18. Barigozzi G, Franchini G, Perdichizzi A (2007) The effect of an upstream ramp on cylindrical and fan-shaped hole film cooling: part I—aerodynamic results. ASME Paper No. GT2007–27077

19. Zhang C, Song YJ, Song LM, Li J, Feng ZP (2017) Experimental investigation for effects of vortex generator height on film cooling property. J Xi'an Xiaotong Univ 51:20–26

20. Zhang C, Wang Z (2018) Effect of the downstream crescent-shaped block height on the flat-plate film flow and cooling performance. J Appl Mech Tech Phys 59:951–961

21. Zhou WW, Hu H (2016) Improvements of film cooling effectiveness by using Barchan dune shaped ramps. Int J Heat Mass Transf 103:443–456

22. Aga V, Mansour M, Abhari RS (2009) Aerothermal performance of streamwise and compound angled pulsating film cooling jets. ASME J Turbomach 131:041015

23. Gräf L, Kleiser L (2014) Film cooling using antikidney vortex pairs: effect of blowing conditions and yaw angle on cooling and losses. ASME J Turbomach 136:011008

24. Baldauf S, Scheurlen M, Schultz A, Wittig S (2002) Correlation of film-cooling effectiveness from thermograhic measurements at enginelike conditions. ASME J Turbomach 124:686–698